

PAPER

Nanocone-based plasmonic metamaterials

To cite this article: R Margoth Córdova-Castro *et al* 2019 *Nanotechnology* **30** 055301

View the [article online](#) for updates and enhancements.



IOP | ebooks™

Bringing you innovative digital publishing with leading voices to create your essential collection of books in STEM research.

Start exploring the collection - download the first chapter of every title for free.

Nanocone-based plasmonic metamaterials

R Margoth Córdova-Castro , Alexey V Krasavin, Mazhar E Nasir, Anatoly V Zayats and Wayne Dickson

Department of Physics and London Centre for Nanotechnology, King's College London, Strand, London, WC2R 2LS, United Kingdom

E-mail: margoth.cordova_castro@kcl.ac.uk

Received 2 August 2018, revised 5 October 2018

Accepted for publication 22 October 2018

Published 6 December 2018



CrossMark

Abstract

Metamaterials and metasurfaces provide unprecedented opportunities for designing light–matter interactions. Optical properties of hyperbolic metamaterials with meta-atoms based on plasmonic nanorods, important in nonlinear optics, sensing and spontaneous emission control, can be tuned by varying geometrical sizes and arrangement of the meta-atoms. At the same time the role of the shape of the meta-atoms forming the array has not been studied. We present the fabrication and optical characterization of metamaterials based on arrays of plasmonic nanocones closely packed at the subwavelength scale. The plasmonic mode structure of the individual nanocones and pronounced coupling effects between them provide multiple degrees of freedom to engineer both the field enhancement and the optical properties of the resulting metamaterials. The metamaterials are fabricated using a scalable manufacturing procedure, allowing mass-production at the centimeter scale. The ultra-sharp cone apex ($\lesssim 2$ nm) and the associated field enhancement provide an extremely high density of electromagnetic hot-spots ($\sim 10^{10}$ cm $^{-2}$). These properties of nanocone-based metamaterials are important for the development of gradient-index metamaterials and in numerous applications in fluorescence enhancement, surface enhanced Raman spectroscopy as well as hot-carrier plasmonics and photocatalysis.

Supplementary material for this article is available [online](#)

Keywords: metamaterials, plasmonics, field enhancement

(Some figures may appear in colour only in the online journal)

Introduction

Individual dielectric and metallic nanoparticles interacting with light give rise to a variety of important phenomena associated with the presence of electromagnetic resonances, defined by the nanostructure geometry, size, material and surrounding medium [1–4]. When they are assembled in an array with the spacing at a subwavelength distances ($\ll \lambda$), the electromagnetic waves perceive the material as a layer of homogeneous medium, namely, a metamaterial which can be described as an effective medium [5–8] by an effective permittivity (and sometimes permeability) arising from the interaction of the coupled ‘meta-atoms’. Such metamaterials display a tunable electromagnetic response that depends on the subwavelength geometry of the constituent meta-atoms and their filling factor in the surrounding dielectric. Metamaterials provide an excellent platform to design optical properties such as negative refraction, subwavelength

imaging, optical cloaking and an enhanced nonlinear response [7–13].

Fabrication of metamaterials operating in the visible spectral range is generally challenging due to the limitations of standard fabrication techniques in terms of both the achievable resolution and the dimensions of the overall nanostructured area. In this regard, the approaches based on self-assembling and self-organization are very beneficial. A particularly useful method is based on electrodeposition into nanoporous anodized aluminum oxide (AAO) templates [14–16], resulting in an array of vertically aligned nanorods. The diameter of the nanorods may be varied from approximately 10 to 200 nm, and their separation from 30 to 500 nm and their length from a few tens of nm to microns [17–20]. This geometrical flexibility is realized by varying the anodization conditions, namely the voltage and/or electrolyte type, which offers control over the diameter and spacing of the pores comprising the AAO template hence enabling the

diameter and spacing of the nanorods to be engineered. Meanwhile, the length of the nanorods may be tuned by controlling the duration of the electrodeposition. All of these parameters provide multiple degrees of freedom to design the optical response of the metamaterial.

Plasmonic metamaterials based on vertically aligned plasmonic nanorod arrays exhibit unusual linear and non-linear optical properties [17–30]. Such metamaterials are anisotropic and below the effective plasma frequency [25], which depends on the diameter of the rods and their periodicity, they exhibit hyperbolic dispersion with different signs of the permittivity for light polarized parallel ($\epsilon_{\parallel} < 0$) and perpendicular ($\epsilon_{\perp} > 0$) to the rod axis [25–29]. In addition to the high field enhancement due to the small separation of the individual nanorods, their highly-dispersive anisotropic optical properties give rise to extraordinary refractive index sensitivity [19], prominent nonlinear optical effects [24] and enhanced spontaneous emission rate near and inside the metamaterial [23].

The optical properties of these metamaterials are determined by both the plasmonic resonances of the individual gold nanorods and the electromagnetic coupling between them [18]. However, despite the flexibility in engineering of the optical properties via the dimensions and separation of the nanorods [20], consideration should be in turn given to the role of the meta-atom shape. Additional flexibility in engineering the metamaterial spectral characteristics, namely the magnitude and spatial distribution of the field enhancement, can be achieved by replacing the cylindrical nanorods in the metamaterial with more complex elements, such as multishell nanorods, nanotubes or coaxial structures [21, 22]. Varying the shape of the constituent nanoparticles not only facilitates greater flexibility in the tuning of metamaterial modes, but also allows further improvements in the field enhancement by taking advantage of nanoscale geometric effects [31–39]. Increased local optical fields present in particles with sharp apexes have been intensely studied due to their importance for enhancing nonlinear effects [33, 34], improving sensing sensitivity to small molecules [35], Raman spectroscopy [36] as well as for hot-carrier generation [37, 38]. The combination of both, metamaterial architecture and the shape effects of their meta-atoms can be highly advantageous for applications where field enhancement is important. This combination can be realized by a metamaterial formed by arrays of sub-wavelength metallic nanocones. The experimental implementation of such a metamaterial requires high resolution fabrication techniques, capable of achieving upright nanocones with sharp apexes uniformly distributed over a macroscopic area.

Here, we present the fabrication and optical characterization of a plasmonic metamaterial based on an array of metallic nanocones, combining an engineered optical response with an extremely high density of optical hot spots. Previously reported arrays of cones fabricated using lithographic [40–43] or chemical [44, 45] methods feature a relatively large cone base (180–700 nm) and separation (200–800 nm) and do not achieve densities for which interaction between nanocones become important so that

metamaterial properties are revealed. For these large cones, the size of the apex was generally not at nanoscopic scales, while ideal (non-rounded) conical structures were considered in the associated numerical studies. Similarly, roughness of the surface of the previously fabricated large cones is in many cases comparable to the overall size of nanocones studied in this paper and becomes important for overall optical properties due to stochastic field localization effects. The metamaterial developed in this work is fabricated using a scalable method, based on ion-etching of electrochemically grown Au nanorods, which provides well defined and smooth nanocones structures. This fabrication technique allows the realization of a novel metamaterial composed of ultra-sharp plasmonic nanocones (cone base ~ 40 – 60 nm, cone apex $\lesssim 2$ nm) closely packed at the subwavelength scale (nanocone density $\sim 10^{10}$ cm $^{-2}$), enabling strongly coupled plasmonic modes as well as high field enhancement. The experimental results are supported by numerical studies performed to understand the nature of the resonances supported by the metamaterial and their relationship to the ultra-sharp cone apex. These simulations also reveal the strong electromagnetic coupling between the nanocones and the high field localization and enhancement at their apexes, and show how these factors strongly depend on the geometry, cone size, and the illumination conditions. The nanocone-based metamaterials exhibit a high density of electromagnetic hotspots important for enhanced spectroscopies, optical nonlinearities and hot-electron properties as well as for the realization of a transition metamaterial to achieve low reflection and high absorption.

Fabrication methods

Nanorod metamaterial fabrication

The details of the fabrication of the initial gold nanorod metamaterial (figure 1(c)) follows a procedure reported previously [14–20]. Briefly, plasmonic nanorod metamaterials were fabricated via Au electrodeposition into nanoporous AAO templates on a glass substrate. An Al film of a 500 nm thickness was deposited on a substrate by magnetron sputtering. The substrate comprises a glass cover slip with a 20 nm-thick adhesive layer of tantalum pentoxide and a 8 nm-thick Au film acting as a weakly conducting layer. Tantalum pentoxide is deposited by sputtering tantalum in a 20% oxygen/80% argon mixture. The porous alumina structures were synthesized by two step-anodization in 0.3 M oxalic acid at 40 V at 1.6 °C. After an initial anodization step, the formed porous layer was removed by etching in a mixed solution of CrO $_3$ (20 g l $^{-1}$) and 3.5% H $_3$ PO $_4$ at 70 °C leaving an ordered, patterned surface. The samples were then subjected to a second anodization step under the same conditions as in the first step and subsequently etched in 30 mM NaOH to tune the diameters of pores from 50 to 60 nm (the etching rate is 2 nm s $^{-1}$). Gold electrodeposition was performed using a three-electrode system and a non-cyanide solution. The length of nanorods was controlled by the electrodeposition

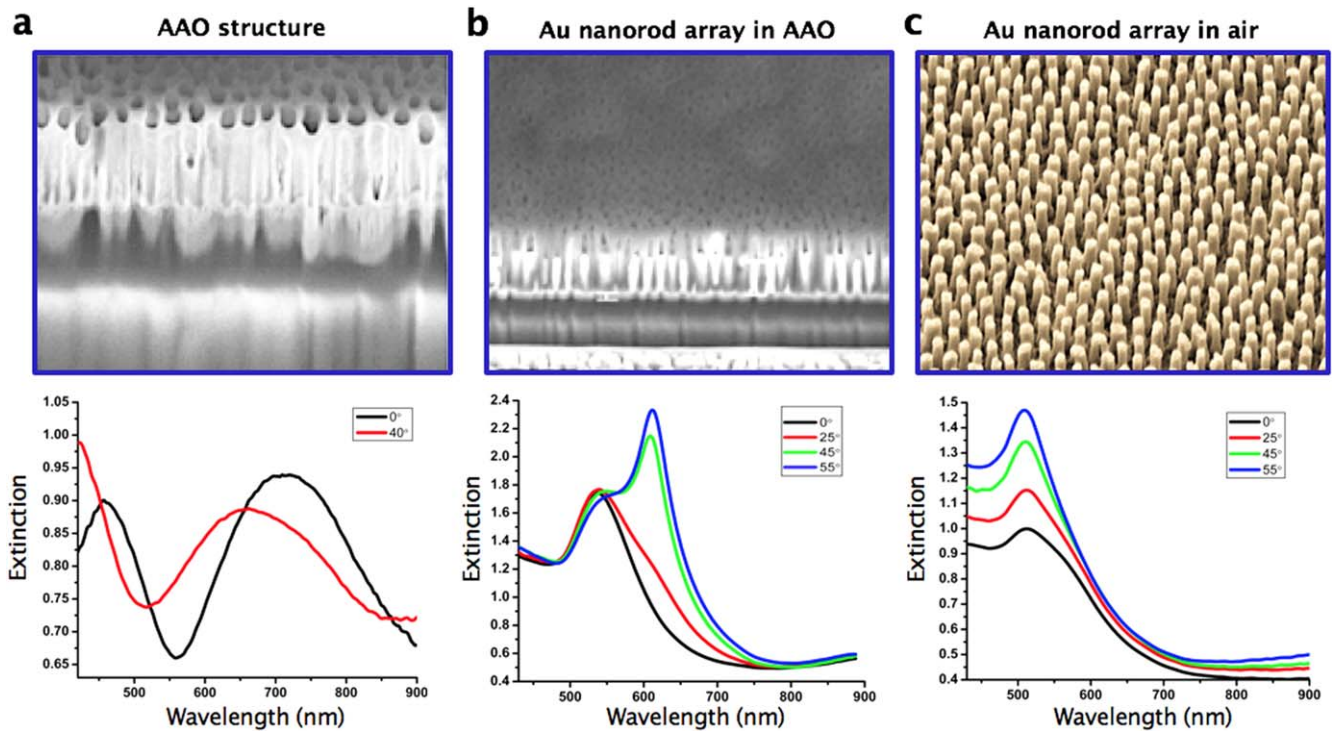


Figure 1. (Top) SEM images and (bottom) measured extinction spectra of *p*-polarized light at different angles of incidence of (a) an oxidized aluminum oxide (alumina, Al_2O_3) template with a hexagonal array of pores (nanopore diameter is 60 nm, the center to center distance is 100 nm, thickness 300 nm), (b) the Au nanorod metamaterial (Au nanorods surrounded by an AAO matrix having a refractive index of 1.66), and (c) the Au metamaterial after the removal of the AAO matrix (Au nanorods in air).

time. Free standing gold nanorod metamaterials were obtained after dissolving the nanoporous alumina template in a mixed solution of 0.3 M NaOH and ethanol.

Nanocone metamaterial fabrication

Arrays of gold nanocones are fabricated by machining arrays of free standing gold nanorods (figure 1) using oblique angle argon ion beam milling (figure 2) [48]. The geometry of the individual nanocones is primarily controlled by varying the ion flux, accelerating voltage, milling duration and the incident angle of the ions.

To create the nanocone metamaterials, it is essential that the gold nanorods are oriented perpendicular to the substrate after the AAO matrix removal (figure 1(c)). Ion-etching of the nanorods is performed using an argon ion beam (figure 2) at an angle of incidence (with respect to the rod axis) of 60° while rotating the substrate at 3 rpm for durations ranging from 60 to 180 s. For all fabricated nanocone samples, the acceleration voltage was 2 kV and the ion beam current was approximately $30 \mu\text{A}$ [45]. The final geometry also strongly depends on the geometrical parameters of the nanorods: the length of the cones is primarily determined by the initial length of the rods, while their sharpness by the power and direction of the Ar ion beam. The shape and size of the nanocones are controlled by varying the duration of the ion etching for a fixed intensity of the ion beam. The length of the nanorod metamaterial is initially determined by the duration of the electrodeposition step (figure 1) however milling at normal incidence to the substrate may be used to decrease the

length of the rods if desired. Depending on the ion-beam intensity profile curvature, the length and diameter of the nanorods and the separation between them, either nanocone or nano-pencil-shaped arrays are created (figure 3).

Figure 2(a) shows a schematic of the Ar ion milling process applied to the nanorod metamaterial. The area of the milling depends on the size of the beam spot which was between 0.5 and 1 cm depending on the beam current and accelerating voltage: a light-colored circular area of nanocones is surrounded by the darker nanorod metamaterial area (figure 2(b)). The scanning electron microscopy (SEM) image presented in figure 2(c) shows the geometry of the nanocone metamaterial after the ion milling of the gold nanorods (110 nm length, diameter 60 nm, center-to-center spacing 100 nm) at an angle of incidence of 60° for 1 min. Using the same parameters to ion-mill rods 240 nm in length results in the nanocone array shown in figure 2(d). In this case, the duration of the ion milling was increased to 180 s to reflect the increased initial length of the nanorods. Using such an oblique angle milling technique, macroscopic areas comprising a nanocone metamaterial with ultra-sharp tips can be fabricated. The area of the final metamaterial is only limited by the size of the incident ion beam with the final structure consisting of an array of parallel nanocones oriented perpendicular to the substrate. The geometry of the individual nanocones can be easily seen in the SEM images in figure 2 with nanocone apexes comparable in dimensions to the resolution limitations of the microscope ($\lesssim 2$ nm). Crucially, it is possible to fabricate large area nanocone

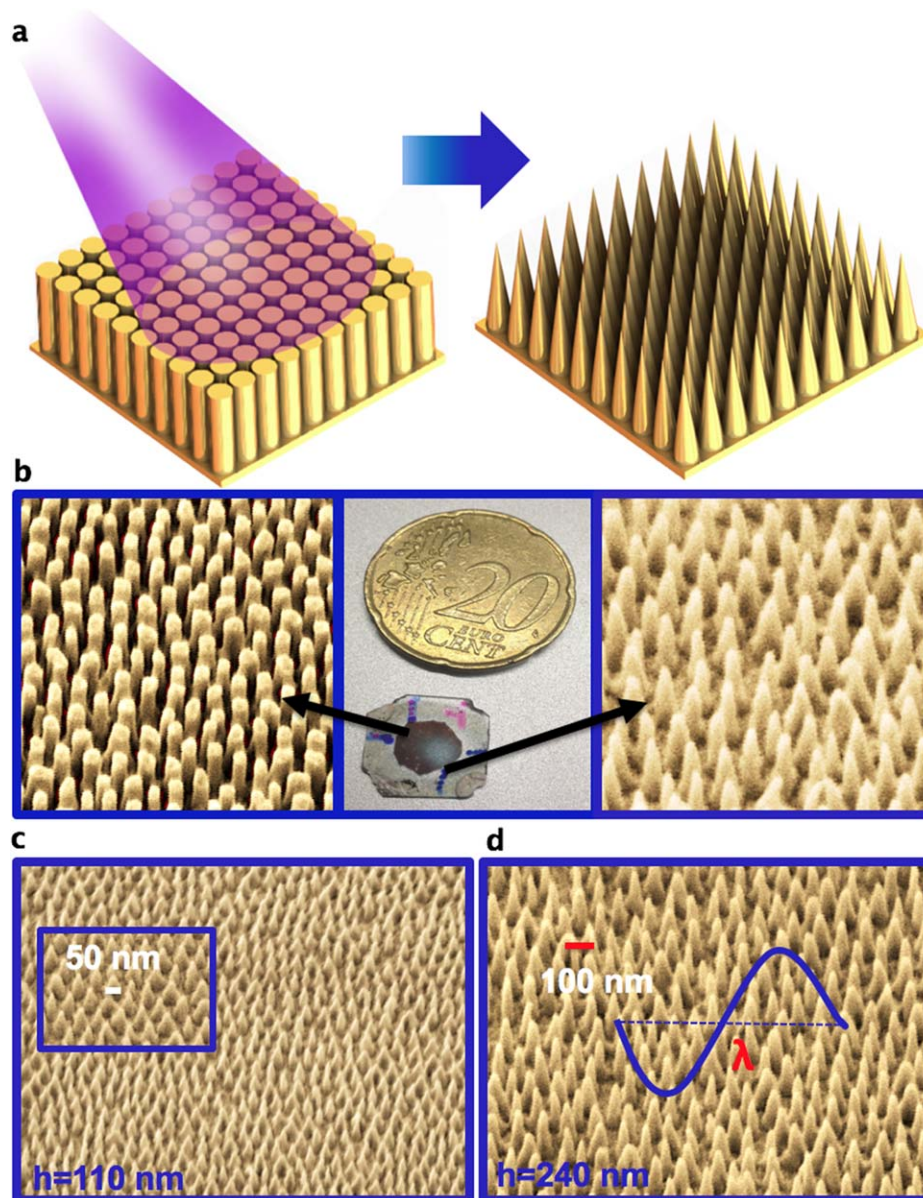


Figure 2. (a) Schematic of Ar ion beam milling at an oblique angle to a nanorod metamaterial in order to fabricate a nanocone metamaterial. (b) SEM images of nanorod- and nanocone-based metamaterials in the same sample, where the ion-etching area of cones in the middle of the sample appears brighter. (c), (d) SEM images of the arrays of the Au nanocones with a base diameter of 60 nm, a 100 nm center to center separation and heights of 110 nm (c) and 240 nm (d).

metamaterials, with ultra-sharp apex diameters and different lengths using a manufacturing-scale fabrication technique. Figure 2(b) also shows that in the nanostructured area, the optical properties change dramatically due to the sensitivity of the plasmonic properties to the nanoscale geometry that manifest in the visible region of the electromagnetic spectra. The area of the nanostructured material with nanorods and nanocones can easily be distinguished by eye. The nanocone region in the center of the sample appears more transparent and colorless, while the nanorod area on the outer side appears in deep red. The area between the nanorods and nanocones is occupied by their intermediate stage, nanopencils. These are produced by the lower intensity at the edges of the argon ion beam.

Optical properties of nanocone metamaterials

Experiment

The measured extinction spectra of the nanorod arrays embedded in an AAO matrix are typical for the considered nanorod parameters [17–20]. For *s*-polarized incident light, there is one extinction peak around 530 nm originating from a transverse plasmonic resonance of the nanorods, while for *p*-polarization at non-zero angles of incidence, another extinction peak appears at around 620 nm in the epsilon near zero regime (figure 1(b)) [28, 29], which can be tuned throughout the visible and near-infrared spectral range by varying the nanorod diameter and period [25–29]. Generally, the position of both peaks depends on the diameter of the nanorods and

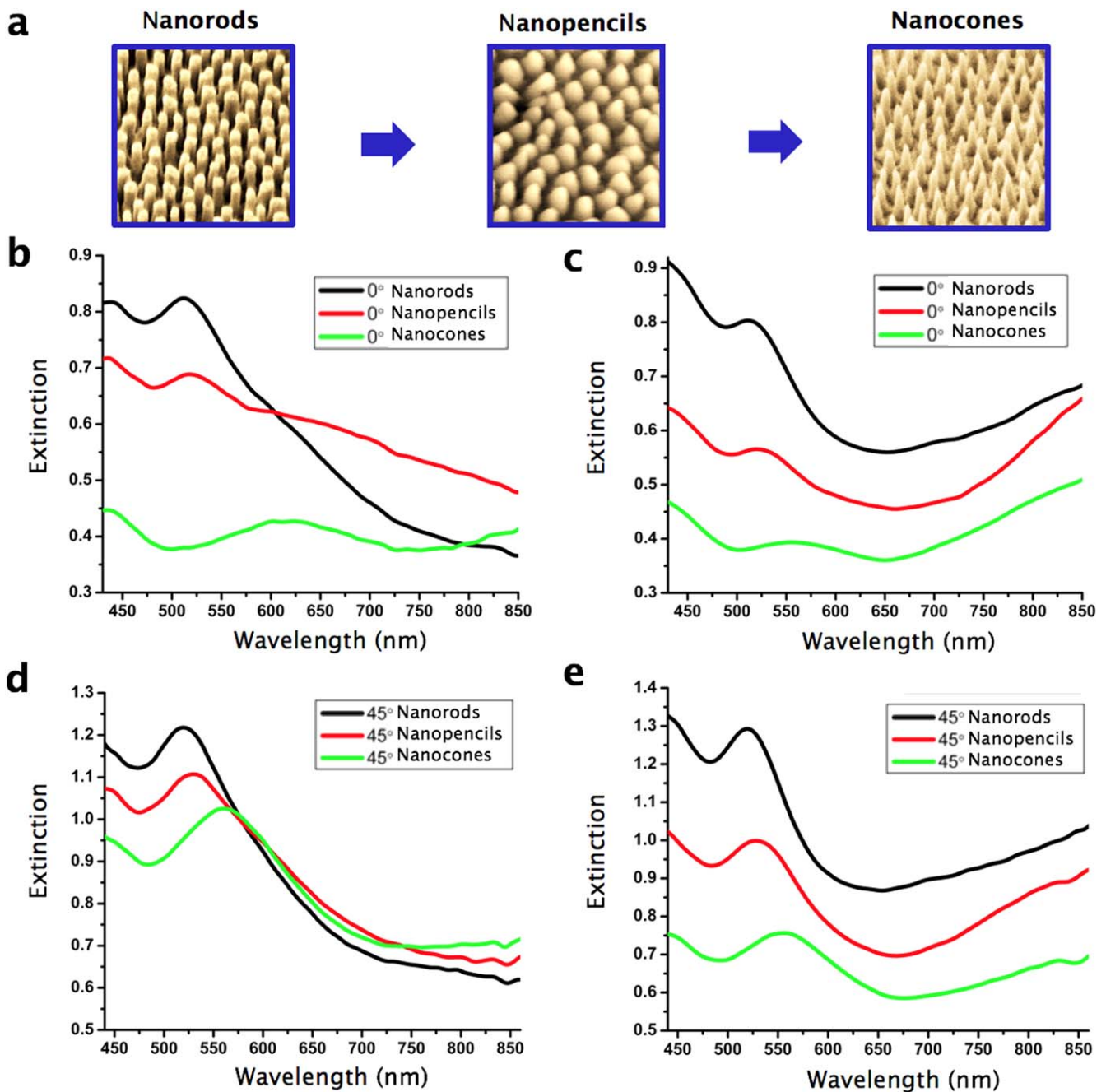


Figure 3. (a) SEM images of the metamaterial during different stages of fabrication. (b)–(e) Extinction spectra measured for nanorod, nanopencil and nanocone metamaterials in air for *p*-polarized illumination at (b), (c) normal and (d), (e) oblique incidence for meta-atoms of (b), (d) 110 nm and (c), (e) 240 nm lengths. For all metamaterials, the meta-atom base diameter is 60 nm and center-to-center separation is 100 nm.

separation between them [26], for instance, by increasing the nano rod separation or introducing a high-index surrounding material allows the effective plasma frequency to be shifted into the near-infrared spectral range [20]. When the alumina matrix (figure 1(b)), having a refractive index of 1.66, is removed and the surrounding medium is air (figure 1(c)), the optical properties change significantly, evidenced by a shift of the long-wavelength extinction peaks which spectrally overlap with the transverse resonance resulting in a broad peak around 510 nm (figure 1(c)). The optical properties of the nanorod, nanopencil and nanocone arrays surrounded by air

are compared in figure 3. When the shape of the meta-atoms changes to sharp cones, extinction peaks at normal and oblique illumination are red-shifted (figure 3). The extinction is markedly lower compared to nanorods, especially for the longest nanorods, while the width of the resonance increases for all nanocone lengths. For the rods with a ~ 110 nm length and a 60 nm diameter, the Ar beam can pass through the structure and the gold layer below the metamaterial is also milled.

Figure 4 shows the comparison of measured extinction spectral curves for the nanorod and nanocone metamaterials

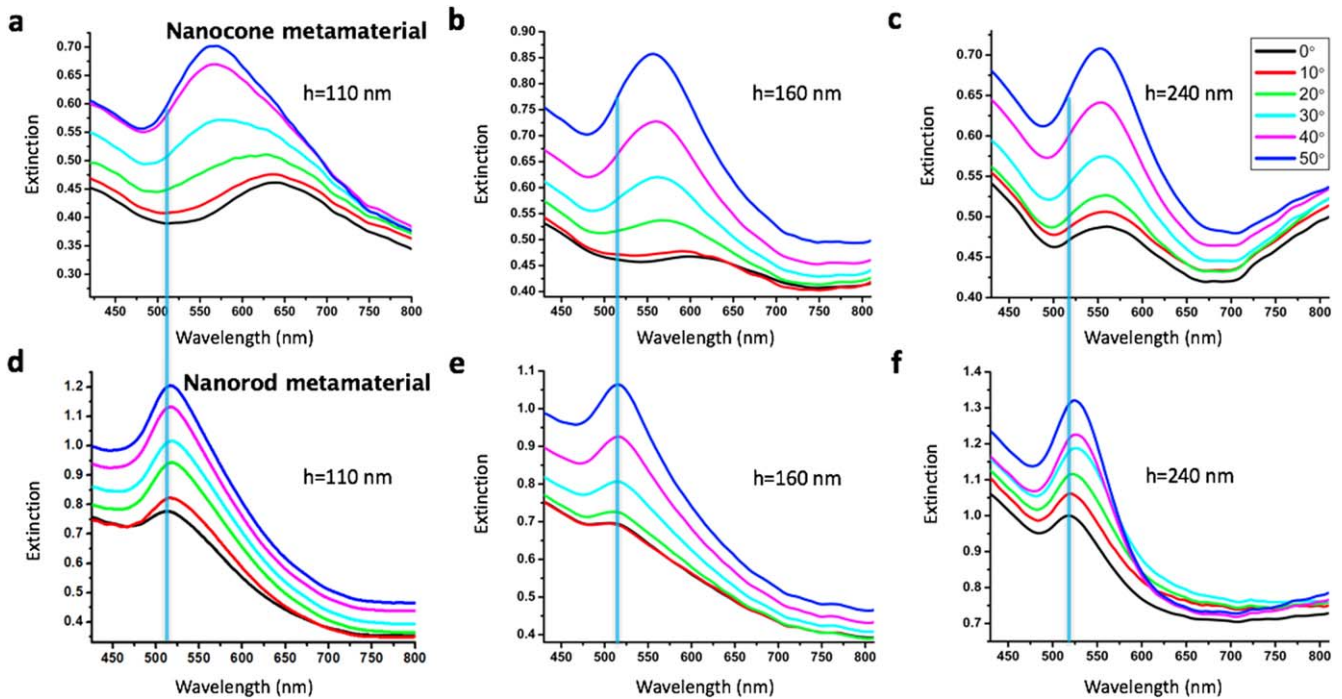


Figure 4. Measured extinction spectra for (a)–(c) nanocone and (d)–(f) nanorod metamaterials in air with a meta-atoms of a 60 nm base diameter and 110 nm (a), (d), 160 nm (b), (e), 240 nm (c), (f) lengths for linearly *p*-polarized light illumination at various incident angles.

of 110, 160 and 240 nm element lengths and illumination from 0° to 50° . Here, the resonance that occurs at normal incidence in nanorods at around 515 nm (figure 4(d)) is observed at a longer wavelength around 630 nm for the short nanocones (figure 4(a)). With the increase of the nanocone height, the effect of separation is diminished, for instance the extinction spectrum for the metamaterial with a 160 nm nanocone length shows that the peak at normal incidence is around 620 nm (figure 4(b)) and for cones with a 240 nm length it is at 560 nm (figure 4(c)). On close inspection of the extinction curves in figure 4(a) (e.g. the cyan curve for 30° illumination), one can observe that there are actually two peaks in the extinction, with the same behavior as in the case of the nanorods in the AAO matrix, suggesting their similar nature.

Numerical modeling

In order to understand the observed optical properties, numerical simulations were initially performed on isolated meta-atoms forming the metamaterials using the discrete dipole approximation [51]. Infinite periodic arrays for both nanorods and nanocones were modeled using finite element numerical simulations [52] taking dielectric constants for gold from [46] with a corrected mean free path of 3 nm [47].

For isolated nanorods and nanocones in air (no substrate) with the illumination along their axes (electric field perpendicular to the axis), the resonances occur at wavelengths of approximately 520 nm and 534 nm, respectively. The calculated near field intensity maps at the resonant wavelength show a typical dipolar plasmonic mode localized along the base of both geometries in direction of the incident

electric field (figures 5(a) and (d)). When the nanoparticle is illuminated from the side so that the electric field is along the meta-atom axes (figures 5(c) and (f)), the peak associated with the electron oscillations along the nanoparticles is present. In the case of nanorod, the resonant peak is at 553 nm with the plasmonic mode localized all around the bases of the rod and exhibiting typical dipolar shape. For the nanocone, the resonant peak occurs at 634 nm and the respective near field intensity map shows the localization of the field in the cone apex while the field intensity increases significantly up to 150 times. For the dimensions considered (aspect ratio ~ 2), the extinction is dominated by absorption and both shapes have similar extinction. At oblique incidence, both resonances are excited (figure 5(b)), for a nanorod, the resonances overlap and a single peak is observed at 556 nm, the extinction efficiency increases by a factor or two and the resonance broadens. The nanocone illuminated at oblique incidence presents well-separated resonances at 540 and 650 nm and the extinction for the transverse resonance remains around 2.5 (figure 5(e)), while the scattering becomes significant for both geometries. The intensity distributions for these cases are presented in figures S1(b) and (c) available online at stacks.iop.org/NANO/30/055301/mmedia. The near field intensity map at oblique incidence for the nanorod at the resonant excitation (figure S1(a)) shows the superposition of transverse and longitudinal dipolar modes.

In the case of strongly interacting nanocones, with separation of 60 nm (figure 5(g)), the extinction spectra at normal incidence illumination show the transverse peak at 560 nm. At oblique incidence, two extinction peaks can be observed the same as for an isolated nanocone, one at 560 nm and another at 765 nm (figure 5(g)). Extinction of the

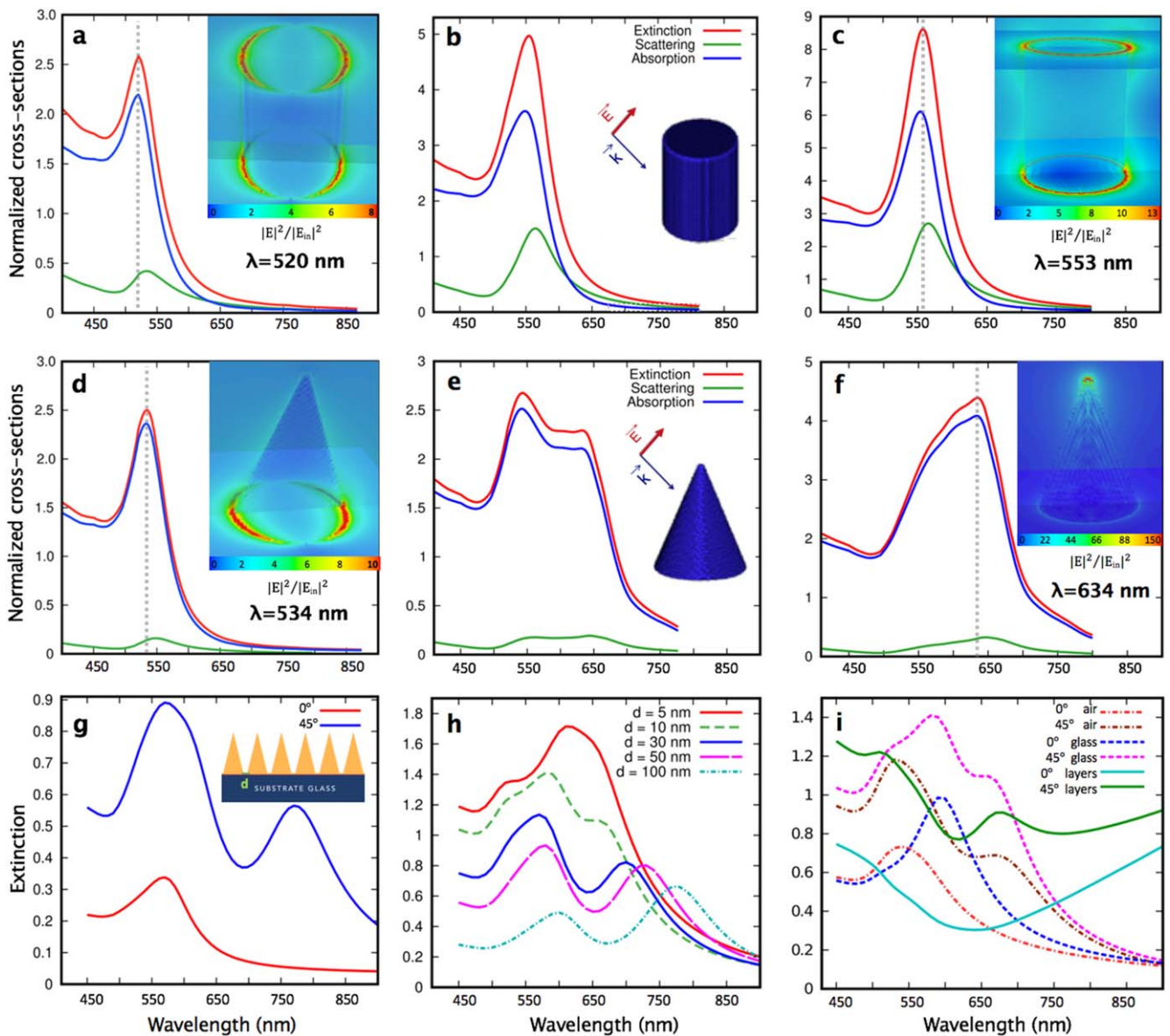


Figure 5. Simulated extinction, absorption and scattering cross-sections normalized by the particle geometrical cross-sectional area for (a)–(c) an isolated nanorod (height 110 nm, diameter 60 nm) and (d)–(f) an isolated nano cone (height 110 nm, base 60 nm, apex radius 2 nm) in air illuminated with a *p*-polarized plane wave at (a,d) 0°, (b,e) 45° and (c,f) 90°. Inserts in (a), (c), (d), (f) are the near-field intensity maps corresponding to the plasmonic resonances as indicated. (g) Calculated extinction spectra for an infinite square array of Au nanocones of a 60 nm base diameter, a 2 nm apex radius and a 110 nm length with a period of 120 nm, supported by a glass substrate; the metamaterial is illuminated with *p*-polarized plane wave at 0° and 45° angles of incidence. (h) Extinction spectra of the nanocone metamaterial illuminated at 45° for various periods. (i) Extinction spectra calculated for a nanocone metamaterial (period 70 nm, all other parameters as in (g)) suspended in air, on a glass substrate and on a glass substrate coated with 20 nm tantalum pentoxide and 8 nm gold underlayers.

transverse mode increases significantly compared to the isolated particles.

The effect of coupling between meta-atoms in the metamaterial can be seen when the individual cones or rods are placed in a square array having a subwavelength periodicity. Figure 5(h) reveals the collective nature of the cone metamaterial modes induced by the coupling between the individual nanocones as demonstrated by the change of the extinction spectra for arrays of cones having different periodicities (ranging from 160 to 65 nm). It can be seen that as the cones become closer with the decrease of the separation from 100 to 30 nm, both modes are blue-shifted, for a 10 nm

separation, three modes are observed and, for 5 nm separation, two of these modes overlap. As observed earlier, the extinction of the structure is highly affected by the presence of the substrate and the underlying Ta₂O₅ and gold layers, which can be seen in figure 5(i) on an example of the same cone array surrounded by air, on glass, and on glass with the underlying layers.

Simulated spectra (figure 6(a)) are in a good agreement with the experiment (figure 4). The calculated extinction spectra for a nanorod metamaterial illuminated at normal incidence show an extinction peak around 516 nm with maximum extinction intensity of 1.1, for oblique illumination

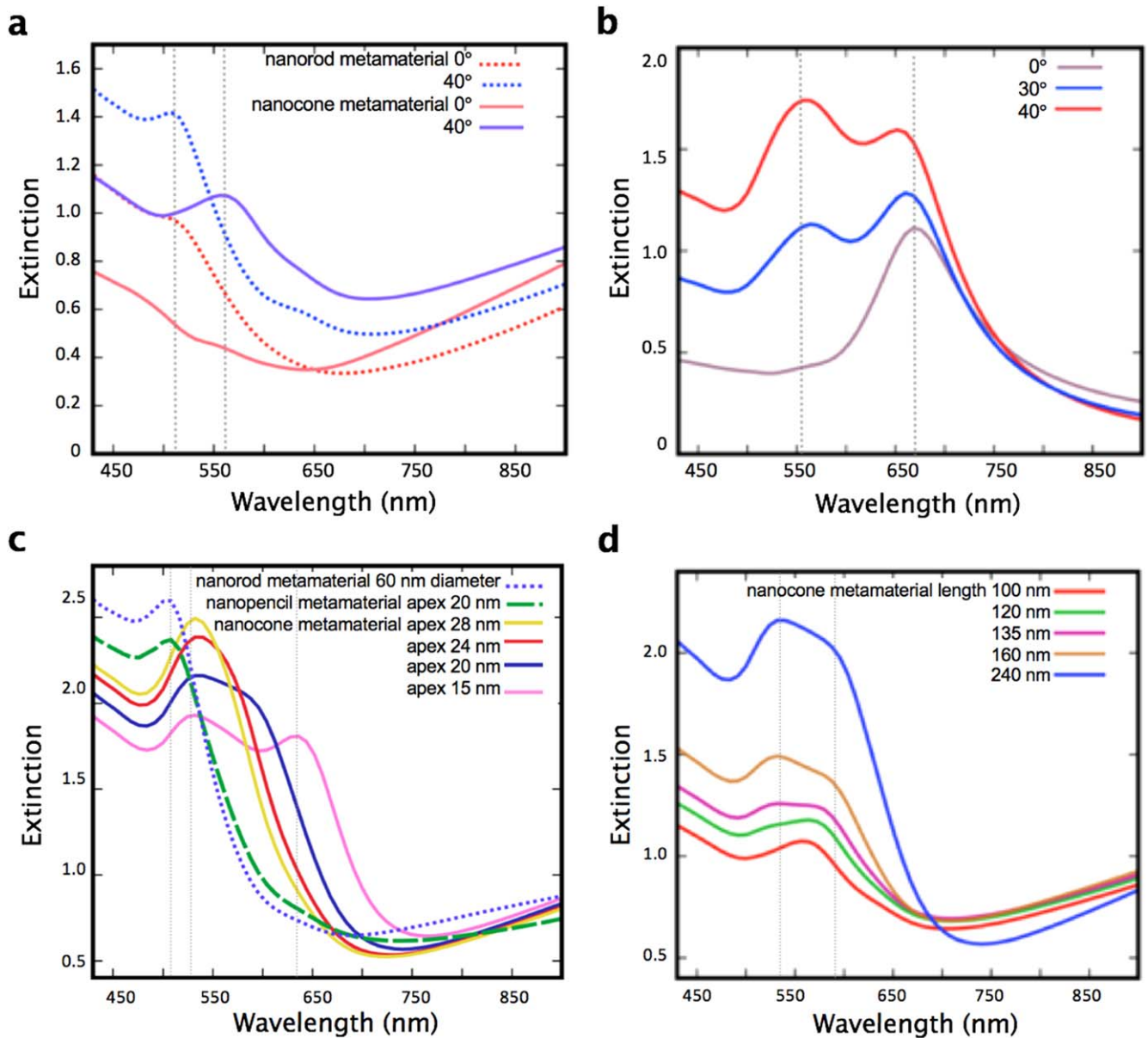


Figure 6. Simulated extinction spectra for various metamaterials: (a) nanorod and nanocone metamaterials (height 110 nm, base 60 nm, cone apex diameter 20 nm) for an infinite square array with a periodicity of 100 nm on a glass substrate with 8 nm gold and 20 nm tantalum pentoxide underlayers; (b) the nanocone metamaterial as in (a) but without the 8 nm Au underlayer; (c) the nanorod metamaterial (60 nm diameter and 240 nm length), the nanopencil metamaterial with the same dimensions and an apex of a 20 nm diameter, and the nanocone metamaterial of the same base diameter and height and various apex diameters between 28 nm and 15 nm; (d) the nanocone metamaterial with different heights of nanocones with a 20 nm apex diameter and a 60 nm base diameter. The metamaterials are in air illuminated with a p -polarized plane wave at 40°, if not specified otherwise.

the maximum intensity of the extinction peak increases to 1.45. For the nanocone metamaterial (cone apex radius of 10 nm), the peak in extinction at normal incidence experiences a red shift to 560 nm and decreases significantly to a value of 0.5. At oblique incidence the peak is also present at around 560 nm and, in comparison with the nanorod metamaterial, the extinction intensity decreases to a value of 1.15. Near-field intensity maps at the wavelength of the maximum in the extinction peak at normal incidence show that the nanorod metamaterial exhibits higher field enhancement than the nanocone metamaterial (see figures S3(a) and (c)). At oblique incidence, the field localization at the apex of the nanocone

meta-atoms (figure 3S(d)) surpasses that in the nanorod arrays (figure 3S(b)) at any incident angle. If the underlying gold layer is removed by the ion milling and nanocones are electrically separated (and being only supported by the tantalum pentoxide layer having a refractive index of around 2.1), the peak at normal incidence is more prominent (figure 6(b)) than with the Au underlayer (figure 6(a)), which leads to the double peak structure observed in short nanocones (figure 4(a)). In figure S2, where the Au underlayer is omitted, the near-field intensity maps show that the mode around 650 nm is localized at the base of the cones with a clear indication of coupling in the array, while there is hardly any field present at the cone

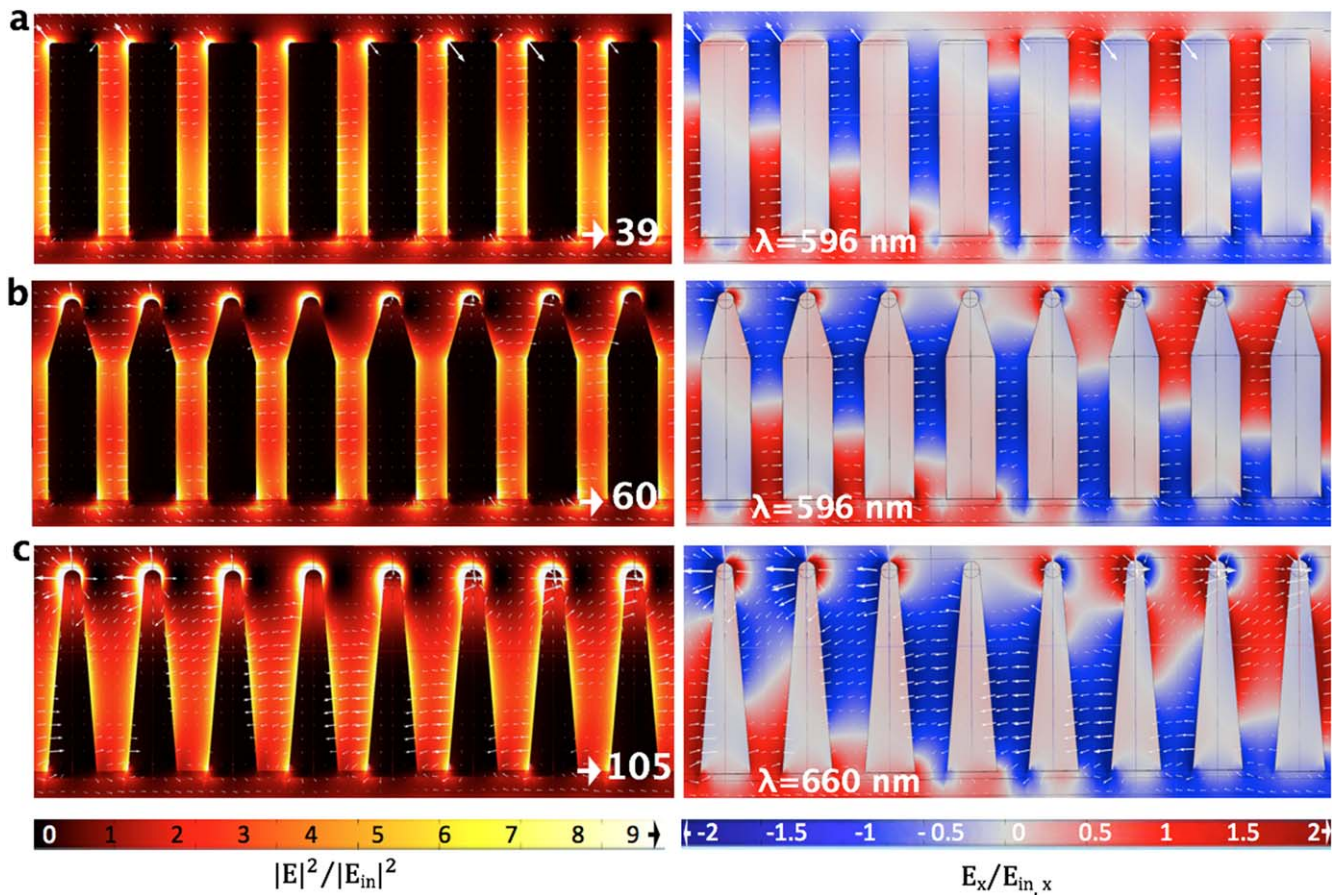


Figure 7. Near field intensity (left) and E_x component of the field (right) for (a) nanorod and (b) nanopencil metamaterials at a 596 nm wavelength and (c) nanocone metamaterial at a 660 nm wavelength. These wavelengths correspond to the maxima of the field enhancement for the respective metamaterials under the illumination with p -polarized light at a 40° angle of incidence. The metamaterials parameters are (a) 60 nm diameter, 240 nm length, (b), (c) 60 nm base diameter, 240 nm length, 10 nm apex radius, in (b) the cylindrical section length is 170 nm. To avoid numerical artefacts and unphysical results, the top edge of the nanorods was rounded with a radius of 5 nm.

apexes in this case. However, at the 550 nm resonance, the maximum of the localized fields is exactly at the apex, with some modal field intensity also present at the base of the cones.

In order to illustrate the effect of the apex on the extinction peak, the calculations for a metamaterial with the nanocones of different apex radii from 14 to 7.5 nm have been carried out, keeping the same base diameter of 60 nm and height of 240 nm (figure 6(c)). Figure 6(c) also shows the calculations of the extinction for nanopencil-like shapes which consists in a combination of the rods at the bottom and a cone of apex radius of 10 nm at the top, such a geometry is fabricated when the ion-beam changes the shape only at the top of the rod (figure 3). It is observed that the peak remains at the same wavelength as for the nanorod metamaterial at 516 nm but with decreased extinction. When the cone shape is completely formed the extinction of the nanocone metamaterial with the same apex radius of 10 nm further decreases, the peak is red-shifted and becomes broader (figure 6(c)).

By comparing the rod and cone meta-atoms of the same diameter and length, one can see that for cones with a 7.5 nm apex radius, the extinction peak is shifted to 540 nm

(figure 6(c)). As the sharpness of the nanocones increases, the extinction decreases and a second peak begins to appear at longer wavelengths, this second peak red shifts for smaller apexes while the peak around 540 nm remains at approximately the same wavelength. The field intensity dramatically increases with only a few nanometer reduction of the apex radii of the cone meta-atoms, increasing by more than 3 times, as can be observed comparing figures S4(d) and S4(f) for 10 and 7.5 nm apex radii, respectively. The near field intensity maps also show that for a 7.5 nm apex radius the two modes that appear at oblique illumination are spectrally well separated (figures S4(e) and (f)). As the length of the cones is increased from 100 to 240 nm while the apex radius is kept constant at 10 nm, the extinction peak becomes broader, significantly increases and is red-shifted from 560 to 600 nm. Meanwhile, a second peak appears around 525 nm (figure 6(d)), the field distributions of the modes are also different for the metamaterials with short and long cones (figures S3 and S4).

In contrast with the isolated meta-atoms, the maximum of the field enhancement in the metamaterials does not correspond to the peak in the extinction (figure 7). Figures S4 and 7 show the field distribution at the wavelengths of the highest

extinction and the highest field enhancement, respectively, for nanorod, nanopencil and nanocone metamaterials. For the nanorod and nanopencil metamaterials, the strongest field enhancement occurs at the wavelength of 596 nm with the corresponding intensity enhanced by a factor of approximately 40 and 60, respectively. For the nanocone metamaterials, this occurs at 660 nm with a 105-fold intensity enhancement. For both nanopencil and nanocone metamaterials, the maximum field enhancement is observed at the apex. The coupling between individual nanostructures in the array can be seen in the electric field distributions. If the length of the cone (figure S5) and the apex diameter (figure S6) decreases, the field enhancement increases significantly.

Conclusions

We have introduced a new metamaterial platform based on arrays of plasmonic nanocones combining both engineered mode dispersion and a very high density of electromagnetic hot spots. Nanocone fabrication by ion beam milling is readily capable of producing large area (cm^2) metamaterials with nanometric dimensions, in keeping with the self-assembled nature of the nanorod precursor material. This technique can be readily adapted to fabricate either arrays of ultra-sharp nanocones or even individual nanostructures from rods which can be made by any standard fabrication technique. Such structures can be used in other applications where the cone shape is essential, e.g. antireflective or hydrophobic materials [43, 48–50].

The nanocone metamaterials introduced in this work cannot be described as a uniform effective layer, as the metal filling factor changes along the cone axis, so that the effective plasma frequency must vary perpendicular to the substrate. A metamaterial with such properties is described as a gradient refractive index layer, also inheriting anisotropic optical properties from the initial nanorod metamaterial. Previous theoretical works introduce for this case the nomenclature of ‘transition metamaterials’ [53–56], in contrast with ordinary metamaterials described as homogeneous media.

Nanocone-based metamaterials featuring coupled electromagnetic modes provide rich optical properties, tunability and high field localization with a high density of electromagnetic hot spots ($\sim 10^{10} \text{ cm}^{-2}$). Together, these properties can lead to enhanced optical functionalities and are, therefore, extremely promising for applications related to enhanced spectroscopies, nonlinear optics, sensing and hot-electron generation.

Acknowledgments

This work has been supported in part by the EPSRC (UK) through Reactive Plasmonics project and the ERC iPLASMM project (321268). RMCC acknowledges support from Mexican National Council of Science and Technology (CONACYT) through doctoral fellowship. AZ acknowledges support from the Royal Society and the Wolfson Foundation.

Author contributions

WD proposed the idea of nanocone metamaterial fabrication using argon ion milling. RMCC developed the method for the nanocone metamaterial fabrication, performed the optical structural and optical characterization and numerical simulations. The manuscript was written through contributions of all authors. All authors have given approval to the final version of the manuscript. All data supporting this research are provided in full in the results section and in the Supplementary Information.

ORCID iDs

R Margoth Córdova-Castro  <https://orcid.org/0000-0003-2420-6399>

References

- [1] Van de Hulst H C 1981 *Light Scattering by Small Particles* (New York: Dover)
- [2] Bohren C F and Huffman D R 1983 *Absorption and Scattering of Light by Small Particles* (New York: Wiley)
- [3] Novotny L and Hecht B 2006 *Principles of Nano-Optics* (New York: Cambridge University Press)
- [4] Maier S A 2007 *Plasmonics: Fundamentals and Applications* (New York: Springer)
- [5] Maxwell Garnett J C 1904 Colours in metal glasses and in metallic films *Philos. Trans. R. Soc. A* **203** 385–420
- [6] Bruggeman D A G 1935 *Ann. Phys.* **416** 636–64
- [7] Engheta N and Ziolkowski R W 2006 *Metamaterials: Physics and Engineering Explorations* (Hoboken, NJ: Wiley)
- [8] Solymar L and Shamonina E 2009 *Waves in Metamaterials* (New York: Oxford University)
- [9] Zhang S, Fan W, Panoui N C, Malloy K J, Osgood R M and Brueck S R 2005 Experimental demonstration of near-infrared negative-index metamaterials *Phys. Rev. Lett.* **95** 137404
- [10] Veselago G 1968 The electrodynamics of substances with simultaneously negative values of ϵ and μ *Sov. Phys. Usp.* **10** 509
- [11] Pendry J B 2000 Negative refraction makes a perfect lens *Phys. Rev. Lett.* **85** 3966
- [12] Pendry J B, Schurig D and Smith D R 2006 Controlling electromagnetic fields *Science* **312** 1780
- [13] Poddubny A, Iorsh I, Belov P and Kivshar Y 2013 Hyperbolic metamaterials *Nat. Photon.* **7** 243
- [14] Masuda H and Fukuda K 1995 Ordered metal nanohole arrays made by a two-step replication of honeycomb structures of anodic alumina *Science* **268** 1466–8
- [15] Li A P, Muller F, Birner A, Nielsch K and Gosele U 1998 Hexagonal pore arrays with a 50–420 nm interpore distance formed by self-organization in anodic alumina *J. Appl. Phys.* **84** 6023
- [16] Ding G Q, Zheng M J, Xu W L and Shen W Z 2005 Fabrication of controllable free-standing ultrathin porous alumina membranes *Nanotechnology* **16** 1285–9
- [17] Evans P, Hendren W R, Atkinson R, Wurtz G A, Dickson W, Zayats A V and Pollard R J 2006 Anisotropic optical properties of arrays of gold nanorods embedded in alumina *Nanotechnology* **17** 5746

- [18] Wurtz G A, Dickson W, O'Connor D, Atkinson R, Hendren W, Evans P, Pollard R and Zayats A V 2008 Guided plasmonic modes in nanorod assemblies: strong electromagnetic coupling regime *Opt. Express* **16** 7460
- [19] Kabashin A V, Evans P, Pastkovsky S, Hendren W, Wurtz G A, Atkinson R, Pollard R, Podolskiy V A and Zayats A V 2009 Plasmonic nanorod metamaterial for biosensing *Nat. Mater.* **8** 867
- [20] Nasir M E, Peruch S, Vasilantonakis N, Wardley W P, Dickson W, Wurtz G A and Zayats A V 2015 Tuning the effective plasma frequency of nanorod metamaterials from visible to telecom wavelengths *Appl. Phys. Lett.* **107** 121110
- [21] Nasir M E, Dickson W, Wurtz G A, Wardley W P and Zayats A V 2014 Hydrogen detected by the naked eye: optical hydrogen gas sensors based on core/shell plasmonic nanorod metamaterials *Adv. Mat.* **26** 3532
- [22] Yakovlev V V, Dickson W, Murphy A, McPhillips J, Pollard R J, Podolskiy V A and Zayats A V 2013 Ultrasensitive non-resonant detection of ultrasound with plasmonic metamaterials *Adv. Mat.* **25** 2351
- [23] Ginzburg P *et al* 2017 Spontaneous emission in non-local materials *Light: Sci. Appl.* **6** e16273
- [24] Neira A D, Oliver N, Nasir M E, Dickson W, Wurtz G A and Zayats A V 2015 Eliminating material constraints for nonlinearity with plasmonic metamaterials *Nat. Commun.* **6** 7757
- [25] Vasilantonakis N, Nasir M E, Dickson W, Wurtz G A and Zayats A V 2015 Bulk plasmon-polaritons in hyperbolic nanorod metamaterial waveguides *Laser Photon. Rev.* **9** 345
- [26] Vasilantonakis N, Wurtz G A, Podolskiy V A and Zayats A V 2015 Refractive index sensing with hyperbolic metamaterials: strategies for biosensing and nonlinearity enhancement *Opt. Express* **23** 14329
- [27] Elser J, Wangberg R, Podolskiy V A and Narimanov E E 2006 Nonlocal effects in effective-medium response of nanolayered metamaterials *Appl. Phys. Lett.* **89** 261102
- [28] Pollard R J, Murphy A, Hendren W R, Evans P R, Atkinson R, Wurtz G A, Zayats A V and Podolskiy V A 2009 Optical nonlocalities and additional waves in epsilon-near-zero metamaterials *Phys. Rev. Lett.* **102** 127405
- [29] Wells B M, Zayats A V and Podolskiy V A 2014 Nonlocal optics of plasmonic nanowire metamaterials *Phys. Rev. B* **89** 035111
- [30] Peruch S, Neira A, Wurtz G A, Wells B, Podolskiy V A and Zayats A V 2017 Geometry defines ultrafast hot-carrier dynamics and kerr nonlinearity in plasmonic metamaterial waveguides and cavities *Adv. Opt. Mater.* **5** 1700299
- [31] Kelly K L, Coronado E, Zhao L L and Schatz G C 2003 The optical properties of metal nanoparticles: the influence of size, shape, and dielectric environment *J. Phys. Chem. B* **107** 60208–3113
- [32] Mishechenko M I, Hovenier J W and Travis L D 2000 *Light Scattering by Nonspherical Particles, Theory, Measurements, and Applications* (New York: Academic)
- [33] Hua Y, Chandra K, Dam D H M, Wiederrecht G P and Odom T W 2015 Shape-dependent nonlinear optical properties of anisotropic gold nanoparticles *J. Phys. Chem. Lett.* **6** 4904–8
- [34] Reichenbach P *et al* 2014 Nonlinear optical point light sources through field enhancement at metallic nanocones *Opt. Express* **22** 15484
- [35] Taylor A B and Zijlstra P 2017 Single-molecule plasmon sensing: current status and future prospects *ACS Sens.* **2** 1103–22
- [36] Lai C H, Wang G A, Ling T K, Wang T J, Chiu P K, Chou Chau Y F, Huang C C and Chiang H P 2017 Near infrared surfaces-enhanced raman scattering based on star-shaped gold/silver nanoparticles and hyperbolic metamaterials *Sci. Rep.* **7** 5446
- [37] Safaei T S, Mepham A, Zheng X, Pang Y, Dinh C-T, Liu M, Sinton D, Kelley S O and Sargent E H 2016 High-density nanosharp microstructures enable efficient CO₂ electroreduction *Nano Lett.* **16** 7224–8
- [38] Cortes E, Xie W, Cambiasso J, Jermyn A S, Sundararaman R, Narang P, Schlucker S and Maier S A 2017 Plasmonic hot electron transport drives nano-localized chemistry *Nat. Commun.* **8** 14880
- [39] Tellez-Limon R, Fevrier M, Apuzzo A, Salas-Montiel R and Blaize S 2017 Numerical analysis of tip-localized surface plasmon resonances in periodic arrays of gold nanowires with triangular cross section *J. Opt. Soc. Am. B* **34** 2147–54
- [40] Das G, Battista E, Manzo G, Causa F, Netti P A and Di Fabrizio E 2015 Large-scale plasmonic nanocones array for spectroscopy detection *ACS Appl. Mater. Interfaces* **7** 23597–604
- [41] Gusak V, Kasemo B and Hagglund C 2014 High aspect ratio plasmonic nanocones for enhanced light absorption in ultrathin amorphous silicon films *J. Phys. Chem. C* **118** 22840–6
- [42] Mehrvar L, Sadeghipari M, Tavassoli S H, Mohajerzadeh S and Fathipour M 2017 Optical and surface enhanced raman scattering properties of Ag modified silicon double nanocone array *Sci. Rep.* **7** 12106
- [43] Lee Y, Lee J, Lee T K, Park J, Ha M, Kwak S K and Ko H 2015 Particle-on film gap plasmons on antireflective ZnO nanocone arrays for molecular-level surface-enhanced raman scattering sensors *ACS Appl. Mater. Interfaces* **7** 26421–9
- [44] Zhao J, Sun W, Sun W, Liu L, Xia X, Quan B, Jin A, Gu C and Li J 2014 Rapid templated fabrication of large-scale, high-density metallic nanocone arrays and sers applications *J. Mater. Chem. C* **2** 9987–92
- [45] Instruction Manual for IM4000 Ion Milling System (Hitachi Technologies Corporation, 2011)
- [46] Johnson P B and Christy R W 1972 Optical constants of the noble metals *Phys. Rev. B* **6** 4370
- [47] Lissberger P H and Nelson R G 1974 Optical properties of thin film Au–MgF₂ cermets *Thin Solid Films* **21** 159
- [48] Yang Q, Zhang X A, Bagal A, Guo W and Chang C-H 2013 Antireflection effects at nanostructured material interfaces and the suppression of thin-film interference *Nanotechnology* **24** 23
- [49] Sondergaard T, Novikov S M, Holmgaard T, Eriksen R L, Beermann J, Han Z, Pedersen K and Bozhevolnyi S I 2012 Plasmonic black gold by adiabatic nanofocusing and absorption of light in ultra-sharp convex grooves *Nat. Commun.* **3** 969
- [50] Raut H K, Ganesh V A, Nair A S and Ramakrishna S 2011 Anti-reflective coatings: a critical, in-depth review *Energy Environ. Sci.* **4** 3779
- [51] Draine B T and Flatau P J 1994 Discrete-dipole approximation for scattering calculations *J. Opt. Soc. Am. A* **11** 1491–9
- [52] COMSOL Multiphysics www.comsol.com
- [53] Kim K, Lee D H and Lim H H 2008 Resonant absorption and mode conversion in a transition layer between positive-index and negative-index media *Opt. Express* **16** 18505–13
- [54] Dalarsson M and Tassin P 2009 Analytical solution for wave propagation through a graded index interface between a right-handed and a left-handed material *Opt. Express* **17** 6747–52
- [55] Sun J, Liu X, Zhou J, Kudyshev Z and Litchinitser N M 2015 Experimental demonstration of anomalous field enhancement in all-dielectric transition magnetic metamaterials *Sci. Rep.* **5** 16154
- [56] Wells B, Kudyshev Z A, Litchinitser N and Podolskiy V A 2017 Nonlocal effects in transition hyperbolic metamaterials *ACS Photonics* **4** 2470–8